2010-01-1573

Gain-Scheduling Integrator-Augmented Sliding-Mode Control of Common-Rail Pressure in Diesel-Dual-Fuel Engine

Withit Chatlatanagulchai and Kittipong Yaovaja
Faculty of Engineering, Kasetsart University

Shinapat Rhienprayoon and Krisada Wannatong
PTT Research and Technology Institute, PTT Public Company Limited

ABSTRACT

Accurate common-rail pressure control is vital to good engine performance and low emission. Injection strategy of diesel-dual-fuel engine varies more greatly with speed and load than its diesel engine predecessor, and so does the common-rail pressure set point. Along with this swift set point change, other control challenges exist; they are speed-and-load variation, model uncertainty, sensor noise, actuator nonlinearity, and pressure disturbance from injection. Traditional control such as the PID was proved to be only marginally effective because of the swift set point change. We proposed integrating an integrator-augmented sliding-mode control with gain scheduling and feed-forward term. The sliding-mode control has fast action and is low sensitive to model uncertainty and disturbance. The augmented integrator ensures zero steady-state error. The gain scheduling handles the speed-and-load variation. The feed-forward term helps with the actuator nonlinearity. The proposed control system was implemented with four-cylindrical diesel-dual-fuel engines on an engine dynamometer and in a prototype pick-up truck, which runs on a chassis dynamometer and in road test. The common-rail pressure was accurately regulated both during the new European driving cycle test and the set point changes test. The proposed method compared favorably with the best-tuned gain-scheduling PID controller.

INTRODUCTION

There are about 300,000 new diesel pick-up trucks sold in Thailand each year. With an approximate shelf life of ten years, about three million diesel pick-up trucks are currently used on the road. With minor engine modifications, instead of using pure diesel, these trucks can possibly replace most of their diesel with compressed natural gas (CNG) as their main fuel to reduce total fuel cost. This modified engine is called diesel-dual-fuel (DDF) engine with CNG normally injected in either intake manifold or cylinders' inlet ports.

The biggest challenge for the DDF engine is the making of its control system. Control of the DDF engine is more difficult than that of the gasoline, the diesel, or the pure CNG engines in that the DDF engine must now handle the mixture of the two different fuels. To achieve high CNG replacement ratio, good performance, and low emissions over all operating ranges of engine speed and load, different injection strategy is required for each operating region.

As a result of having various injection strategies, common-rail pressure has been an important factor affecting performance and emissions of the DDF engine. In our well-tuned map of the desired common-rail pressure, presented later in the paper, we saw as much as 100 MPa pressure variations. This wide range of the desired common-rail pressure puts more burdens to the control system. Especially, during transients, when driver quickly demands different engine speed and load, a more elaborate control system that can act quicker than the traditional PID controller is needed.

Control of the common-rail pressure is challenging due to several reasons. First, it is well known that a hydraulic solenoid actuator has unknown and time-varying dead zone and hysteresis. The control system must cancel these hard nonlinearities either using the inverses of their mathematical models or using feed-forward term. Second, since the cancellation is almost always imperfect and the engine has wide operating range, it is difficult to obtain accurate plant model that is suitable for control design. Because the engine is to be operated in different environments, this plant model also varies with time. Third, external disturbances do exist, most notably the battery voltage and the fuel temperature variations. There is also small time delay due to the nature of liquid inside the common rail and connecting hose. Being in mass production, low-cost pressure sensor also contains noise.

Existing literature focuses on detailed models to predict the common-rail system behavior. Ref. [1] developed a very detailed model for a common-rail system. The model was proved to match the experiment quite well. However, their model comprises some partial-differential equations, which are not appropriate for control design. Ref. [2] presented a common-rail system model based on energy principle. The model was shown to match an experiment quite closely. No attempt has been made to design controller. Ref. [3] and [4] discussed pressure fluctuations and formulated a detailed model of the common-rail system. No attempt has been made to design controller.

Very few contain control-oriented models. Ref. [5] presented a control-oriented common-rail-system model, developed from physical laws. The model is simplified yet still nonlinear. The sliding-mode control is used for tracking. However, the signum function in the control law can cause excessive control shattering, and stability is not always guaranteed. Ref. [6] proposed a hybrid model, with discrete and continuous interactions, of a common-rail system and showed that, with PID control, the proposed model delivered better tracking performance than the traditional mean-value model. Ref. [7] used single neuron adaptive PID controller to control common-rail pressure of the diesel engine by controlling the overflow valve. Ref. [8] obtained a simple second-order common-rail model and applied a common-rail pressure tracking controller based on quantitative feedback theory to a one-cylinder test bed.

In this paper, we used a control system based on sliding-mode control method presented in [9]. Two advantages of using this method are its order-reduction property and its robustness against plant uncertainty and disturbances. Sliding-mode control has two phases: reaching and sliding phases. During the reaching phase, a fast-switching control law is used to bring the error trajectory to a sliding surface and maintain it there. Once on the sliding surface, the error trajectory will move toward the origin. The sliding surface dynamic is independent of the plant model and the disturbance, which makes the control law robust.

Our proposed control system consists of a sliding-mode controller, an augmented integrator, a dead zone compensator, and a gain scheduler. The sliding-mode controller provides robustness against plant model uncertainty and external disturbances and also contains fast-switching control action. In implementation, augmenting an integrator ensures low steady-state tracking error. The dead zone compensator cancels the effect of the hard nonlinearities so that a linear controller can achieve good performance. The gain scheduler is required to choose the most appropriate set of controller gains when the engine is operated in different speed and load regions.

The proposed control system was implemented with two DDF engines, in which the CNG is injected at the cylinders' inlet ports. One engine was connected with an engine dynamometer and was used as a test bed. The other engine was assembled in a pickup truck and was used on a chassis dynamometer and on the road in actual road tests. A best-tuned PID controller with gain scheduling was used as a base line to compare with the proposed control system.

The experimental results in following the new European driving cycle, in following step reference changes, and of actual road tests have shown excellent tracking performance of the proposed control system compared to the PID controller.

The content of this paper is divided into four sections, which are introduction, control system design, experimental results, and conclusions. We have presented the introduction in this section. In control system design section to follow, we present designs of the gain-scheduling PID controller and the gain-scheduling integrator-augmented sliding-mode controller. The PID controller is used as a baseline for comparing with our proposed sliding-mode controller. Then, in the experimental results section, various implementation results on a pick-up truck and an engine test bed are presented. The paper is closed with a conclusions section followed by all the necessary back matters.

CONTROL SYSTEM DESIGN

Figure 1 is a simplified diagram of diesel engine's common-rail system. A pump supplies high-pressure diesel fuel to the common rail. Inside of the pump, a metering unit houses a plunger gate. The lift of the plunger gate determines how much fuel is delivered. The amount of lift is controlled by varying the duty cycle of a PWM signal sent to the plunger gate's solenoid by the ECU. A pressure sensor senses the pressure inside the common rail. There is a relief valve to prevent over-pressure. Diesel injectors inject diesel fuel into cylinders.

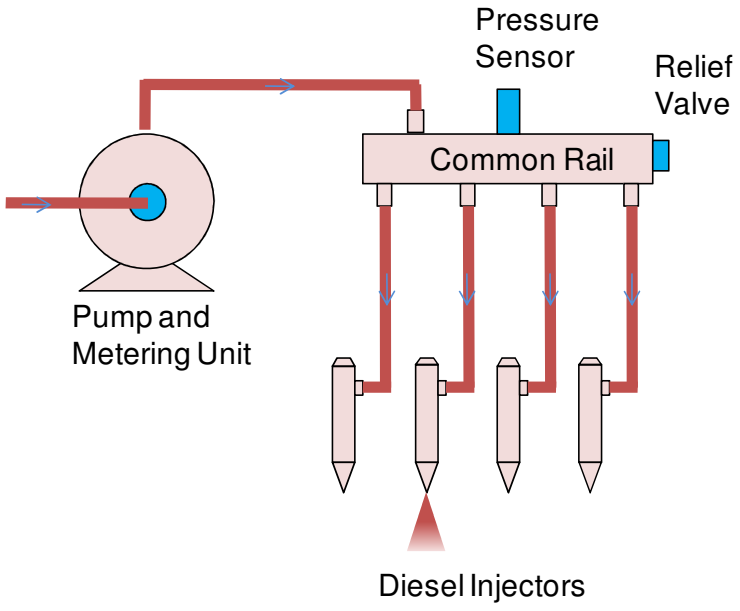

Figure 1: A simplified diagram of common-rail system.

The control objective is to track desired common-rail pressure P_d as close as possible especially during swift changes like in transients. Unlike the diesel engine, the DDF engine has many operating characteristics or zones

that vary with engine speed and load. For example, during low load, only diesel is used for low emissions. For low-to-medium load, DDF mode is used with cylinder skipping for good combustion. For medium and high loads, different replacement ratios are used. This variation in operating characteristics results in extensive range of the desired common-rail pressure. Figure 2 contains a map of the desired common-rail pressure of our DDF engine, as a function of engine speed and torque. The map was tuned during calibration to obtain good performance and low emissions. The desired common-rail pressure has an extensive range of 30 to 130 MPa over the working ranges of the engine speed and torque. As a result, the control system must be able to follow this quick change in the desired pressure, especially when under transient operations.

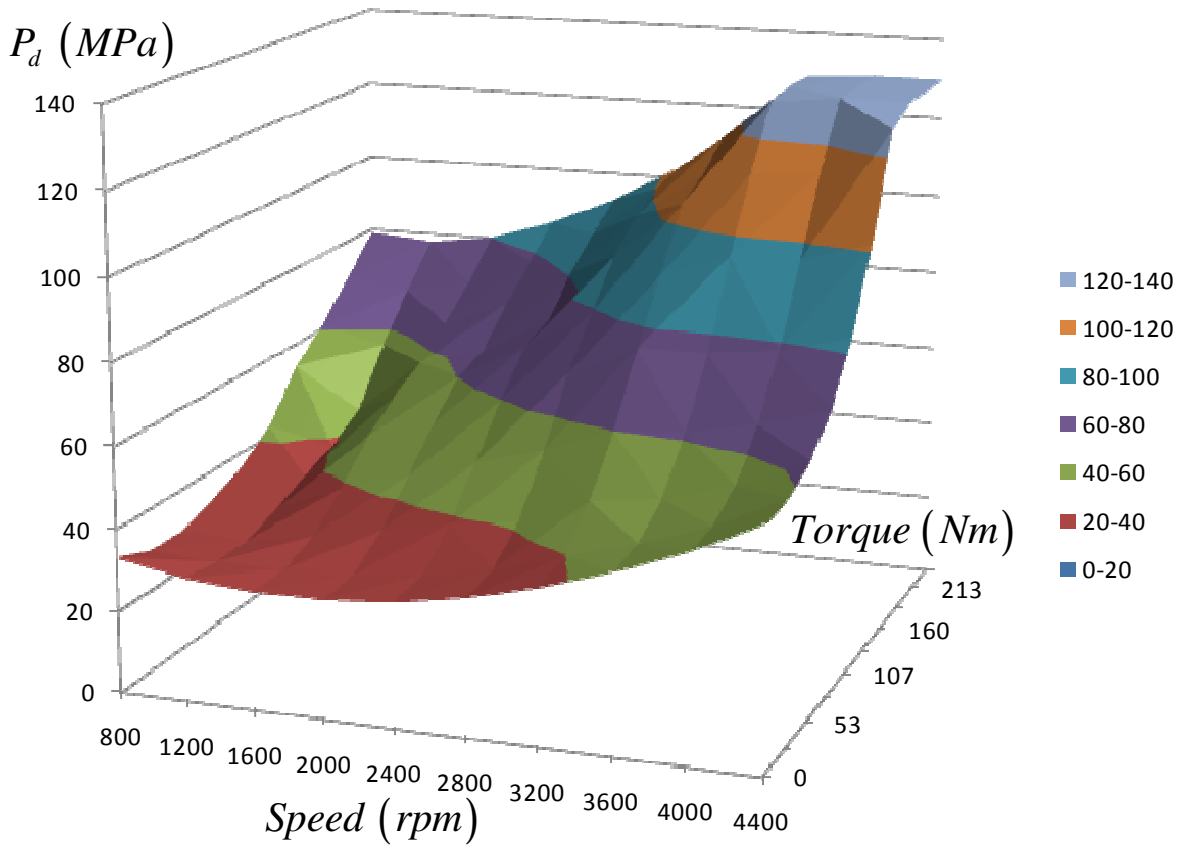

Figure 2: Map of the desired common-rail pressure as a function of engine speed (rpm) and torque (Nm.)

Figure 3 shows our overall control system. Here, plant is a relationship from the solenoid's PWM duty-cycle percentage u to the measured pressure inside the common rail p. p_d is the desired pressure obtained from the map in Figure 2. The error $e = p_d - p$ is fed to the controller to be used in the algorithm.

It is well-known that the hydraulic solenoid has dead zone [10], that is, the insensitivity of an actuator to small input. Our dead-zone compensator is a map, obtained during calibration, as a function of engine speed and torque. The dead-zone compensator outputs a signal u_c, which is the minimum amount of PWM duty cycle to start lifting the plunger gate. Note that this u_c tries to cancel the deadzone effect as much as possible so that a linear controller can achieve good performance.

Due to the extensive ranges of our operating points and desired rail pressure, our controller's gains were tuned also as a function of engine speed and torque, the so-called gain-scheduling scheme. This is to ensure good performance over all working ranges. The output from the controller is u_s.

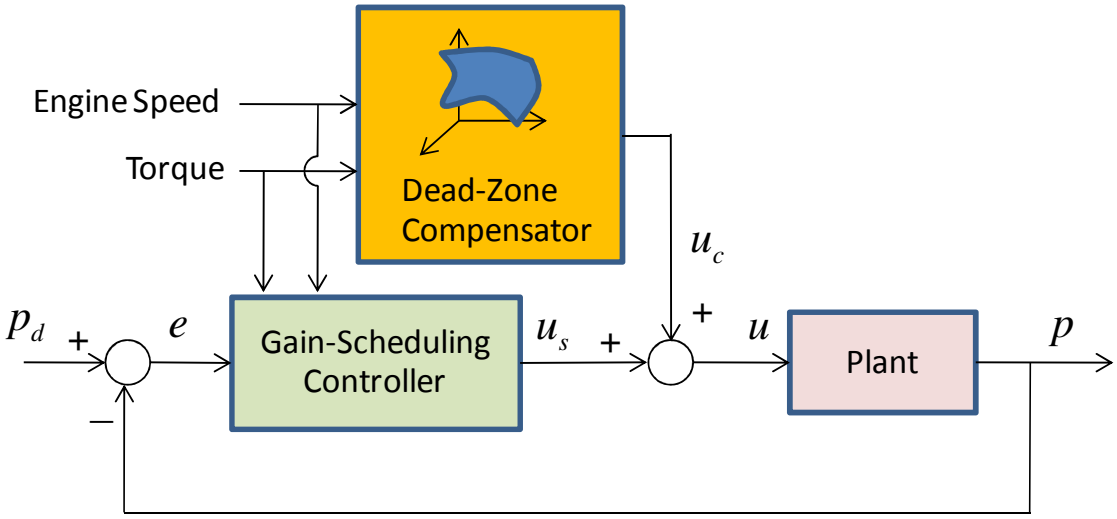

Figure 3: Overall control system with gain-scheduling controller and dead zone compensator.

In this paper, we propose a control system based on the sliding mode control technique. For comparison, however, a PID controller was also implemented. In the following subsection, we briefly discuss the PID controller used.

PID CONTROLLER

We used a standard PID controller in the form

$$u_s = k_p e + k_i \int_0^t e\, dt + k_d \frac{de}{dt}, \tag{1}$$

where k_p, k_i, k_d are proportional, integral, and derivative gains. In transfer function, the PID controller is

$$U_s(s) = \frac{k_d s^2 + k_p s + k_i}{s} E(s),$$

which is improper. So, we appended a low-pass filter $1/(0.1s+1)$ to the PID controller to make it bi-proper.

Figure 4 presents maps of the dead-zone compensator output u_c and the PID gains $k_p, k_i,$ and k_d as functions of engine speed and torque. These maps were obtained during calibration on an engine test bed by fixing an engine speed and torque and inputting a step desired pressure p_d from 30 to 60 MPa. For each operating point, the PID gains were selected to give the best transient response. u_c was selected, for each operating point, as a minimum PWM duty cycle percentage that started lifting the plunger gate (when the measured pressure p started to increase.)

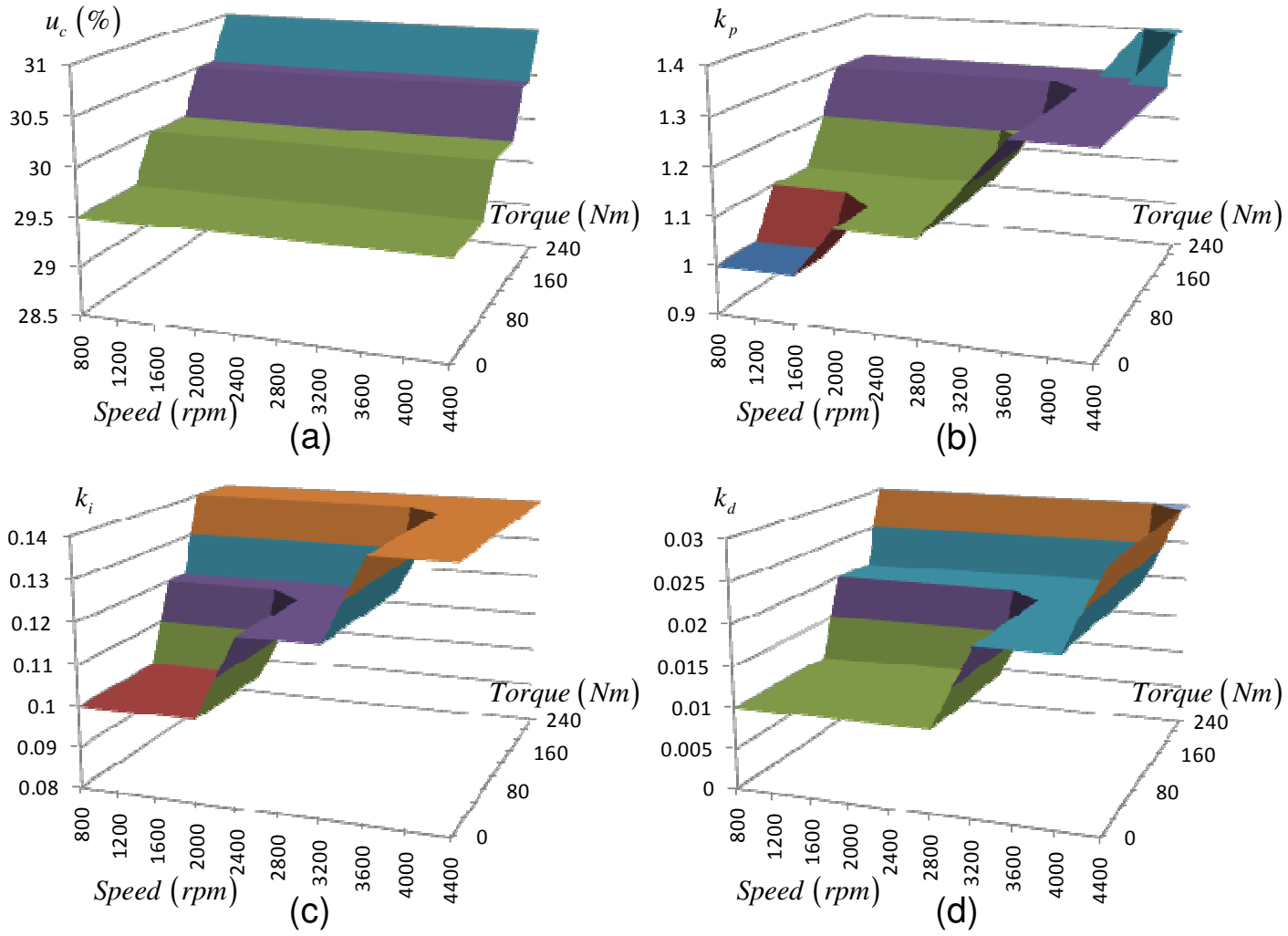

Figure 4: Several maps of design parameters in the PID control system. (a) Dead zone compensator output u_c. (b) Proportional gain k_p. (c) Integral gain k_i. (d) Derivative gain k_d.

In the following subsection, we discuss, in details, a controller based on the sliding-mode control method.

SLIDING MODE CONTROLLER

The sliding-mode controller is model-free, that is, no plant model is required in the control algorithm. However, an upper bound on the plant model functions is required to determine a design parameter. Therefore, we start this section with finding a common-rail state-space model.

Common-Rail Model

A random PWM duty cycle percentage u was passed into the plant in Figure 3. The measured pressure p was recorded, and the pair u, p were used to find the plant transfer function using the command *ident* in Matlab. The means of u and p were first removed to take away the effect of the dead-zone compensator output u_c and

its corresponding pressure output p_c. Therefore, the resulting transfer function represents a relationship from the controller output u_s and its corresponding pressure output p_s.

The plant's second-order transfer function is given by

$$\frac{P_s(s)}{U_s(s)} = \frac{16.02}{0.2297s^2 + 1.181s + 1},$$

whose state-space model is

$$\begin{bmatrix} \dot{\bar{x}}_1 \\ \dot{\bar{x}}_2 \end{bmatrix} = \begin{bmatrix} 0 & 1 \\ -4.35 & -5.14 \end{bmatrix} \begin{bmatrix} \bar{x}_1 \\ \bar{x}_2 \end{bmatrix} + \begin{bmatrix} 0 \\ 1 \end{bmatrix} u_s,$$
$$p_s = \begin{bmatrix} 69.75 & 0 \end{bmatrix} \begin{bmatrix} \bar{x}_1 \\ \bar{x}_2 \end{bmatrix}.$$

Defining $\bar{u}_s = 69.75u_s$, $x_1 = 69.75\bar{x}_1$, and $x_2 = 69.75\bar{x}_2$, we have

$$\begin{aligned} \dot{x}_1 &= x_2, \\ \dot{x}_2 &= -4.35x_1 - 5.14x_2 + \bar{u}_s, \\ p_s &= x_1. \end{aligned}$$

Now we are ready to formulate the tracking problem.

Tracking Problem

Let p_{ds} be desired common-rail pressure for p_s. Note that p_{ds} can be thought of as the desired pressure p_d in Figure 2 subtracted by the corresponding pressure output of the dead-zone compensator p_c. Defining $e_1 = p_s - p_{ds}$ and $e_2 = \dot{p}_s - \dot{p}_{ds}$, we have

$$\begin{aligned} \dot{e}_1 &= e_2, \\ \dot{e}_2 &= -4.35e_1 - 5.14e_2 + \bar{u}_s + \left(-4.35\,p_{ds} - 5.14\,\dot{p}_{ds} - \ddot{p}_{ds}\right). \end{aligned} \tag{2}$$

So, the tracking problem becomes designing $\bar{u}_s$ to drive e_1 and e_2 to zeros. We can achieve this by considering sliding phase and reaching phase.

Sliding Phase and Reaching Phase

Sliding mode control involves two phases: sliding and reaching phases. In the sliding phase, suppose we can design a control law that constrains the trajectories of e_1 and e_2 in (2) to a surface

$$s = a_1e_1 + e_2 = 0.$$

On this surface, the motion is governed by $\dot{e}_1 = -a_1 e_1$. Choosing $a_1 > 0$ ensures that $e_1(t)$ and $e_2(t)$ convert to zeros as time t tends to infinity, and the rate of convergence can be adjusted by adjusting a_1. Note that the motion on the surface $s = 0$ is independent of plant parameters in (2).

In the reaching phase, we need to bring the trajectories of e_1 and e_2 to the surface $s = 0$ and maintain it there. Since

$$\dot{s} = a_1 \dot{e}_1 + \dot{e}_2 = a_1 e_2 - 4.35 e_1 - 5.14 e_2 + \bar{u}_s + \left(-4.35 p_{ds} - 5.14 \dot{p}_{ds} - \ddot{p}_{ds}\right),$$

suppose the desired pressure p_{ds} and its derivatives satisfy the inequality

$$\left|a_1 e_2 - 4.35 e_1 - 5.14 e_2 + \left(-4.35 p_{ds} - 5.14 \dot{p}_{ds} - \ddot{p}_{ds}\right)\right| = \left|a_1 e_2 + h(e_1, e_2)\right| \le \rho(e_1, e_2), \ \forall e_1, e_2 \in R, \qquad (3)$$

for a known function $\rho(e_1, e_2)$, with $V = (1/2)s^2$ as a Lyapunov function candidate, we have

$$\dot{V} = s\dot{s} = s\left[a_1 e_2 + h(e_1, e_2)\right] + s\bar{u}_s \le |s|\rho(e_1, e_2) + s\bar{u}_s.$$

Taking

$$\bar{u}_s = -\beta(e_1, e_2)\,\mathrm{sgn}(s), \qquad (4)$$

where $\beta(e_1, e_2) \ge \rho(e_1, e_2) + \beta_0, \beta_0 > 0,$ and the signum function

$$\mathrm{sgn}(s) = \begin{cases} 1, & s > 0 \\ 0, & s = 0 \\ -1, & s < 0 \end{cases},$$

yields $\dot{V} \le |s|\rho(e_1, e_2) - \left[\rho(e_1, e_2) + \beta_0\right] s\,\mathrm{sgn}(s) = -\beta_0 |s|$. Thus, $W = \sqrt{V} = |s|/\sqrt{2}$ satisfies the differential inequality $D^+ W \le -\beta_0/\sqrt{2}$ and, from the comparison lemma [11], we have $W(s(t)) \le W(s(0)) - \beta_0 t/\sqrt{2}$. Therefore, the trajectories of e_1 and e_2 reach the surface $s = 0$ in finite time and, once on the surface, they cannot leave it, as seen from the inequality $\dot{V} \le -\beta_0 |s|$.

The control law (4) brings the trajectories of e_1 and e_2 to the surface $s = 0$ and maintains it there. However, nothing can be concluded about the bounds of e_1 and e_2 until we further investigate the region of attraction.

Region of Attraction

Suppose (3) becomes $\left|a_1 e_2 + h(e_1, e_2)\right| \le k_1, \ \forall e_1, e_2 \in \Omega,$ where Ω is the region of attraction, for some known nonnegative constant k_1. We can take $\bar{u}_s = -k\,\mathrm{sgn}(s), \ k > k_1$. The condition $s\dot{s} \le 0$ in the set $\{|s| \le c\}$ makes it positively invariant. From $\dot{e}_1 = e_2 = -a_1 e_1 + s$ and the function $V_1 = (1/2)e_1^2$, we have

$$\dot{V}_1 = e_1\dot{e}_1 = -a_1e_1^2 + e_1 s \le -a_1e_1^2 + |e_1|c \le 0, \ \forall |e_1| \ge c/a_1.$$

Thus, $|e_1(0)| \le c/a_1 \Rightarrow |e_1(t)| \le c/a_1, \ \forall t \ge 0$ and the set $\Omega = \{|x_1| \le c/a_1, |s| \le c\}$ is positively invariant.

Since the control law (4) contains the discontinuous signum function, control chattering will occur as a result of imperfection in switching devices and delays. Next, we present two schemes for reducing or eliminating control chattering.

Chattering

The first scheme divides the control law into continuous and switching components to reduce the amplitude of the switching one. Let $\hat{h}(e_1, e_2)$ be an estimate of $h(e_1, e_2)$ in (3). Taking $\bar{u}_s = -\left[a_1e_2 + \hat{h}(e_1, e_2)\right] + v$ yields $\dot{s} = h(e_1, e_2) - \hat{h}(e_1, e_2) + v \le \delta(e_1, e_2) + v$. We can choose $v = -\bar{\beta}(e_1, e_2)\text{sgn}(s)$, where $\bar{\beta}(e_1, e_2) \ge \delta(e_1, e_2) + \bar{\beta}_0, \bar{\beta}_0 > 0$. $\delta(e_1, e_2)$ is an upper bound of the perturbation term and is likely to be smaller than the upper bound $\rho(e_1, e_2)$ of the whole term, hence, reducing chattering.

The second scheme replaces the discontinuous signum function with a continuous arctan function

$$\bar{u}_s = -k(2/\pi)\arctan(s/\varepsilon), \tag{5}$$

where ε is a small number. The smaller the ε is, the closer the arctan function is to the signum function and the more control chattering results.

Using continuous arctan function is a convenient way to prevent control chattering, however, the error trajectories e_1 and e_2 will not go to zeros, but will be ultimately bounded. This proof can be seen in [11]. To obtain zero steady-state errors, an integrator can be augmented to the system as detailed next.

Integral Augmented

Let $e_0 = \int e_1 \, dt$. The augmented system becomes

$$\begin{aligned}
\dot{e}_0 &= e_1, \\
\dot{e}_1 &= e_2, \\
\dot{e}_2 &= -4.35e_1 - 5.14e_2 + \bar{u}_s + (-4.35p_{ds} - 5.14\dot{p}_{ds} - \ddot{p}_{ds}).
\end{aligned}$$

We can then choose

$$s = a_0e_0 + a_1e_1 + e_2, \tag{6}$$

where the matrix $A_0 = [0, 1; -a_0, -a_1]$ is Hurwitz.

In summary, our control law is (5), where s is given by (6). There are then four design parameters: k, ε, a_0, and a_1.

Gain Scheduling

Due to extensive range of the desired pressure p_d in the DDF engine and variety of operating points in terms of engine speed and torque, the four design parameters were obtained during calibration on an engine test bed by fixing an engine speed and torque and inputting a step desired pressure p_d from 30 to 60 MPa. For each operating point, the four gains were selected to give the best transient response. Figure 5 presents maps of the four gains in the sliding-mode control system. In Figure 3, the control input u_s is obtained from $u_s = \bar{u}_s / 69.75$. The compensator input u_c is the same as that in Figure 4(a).

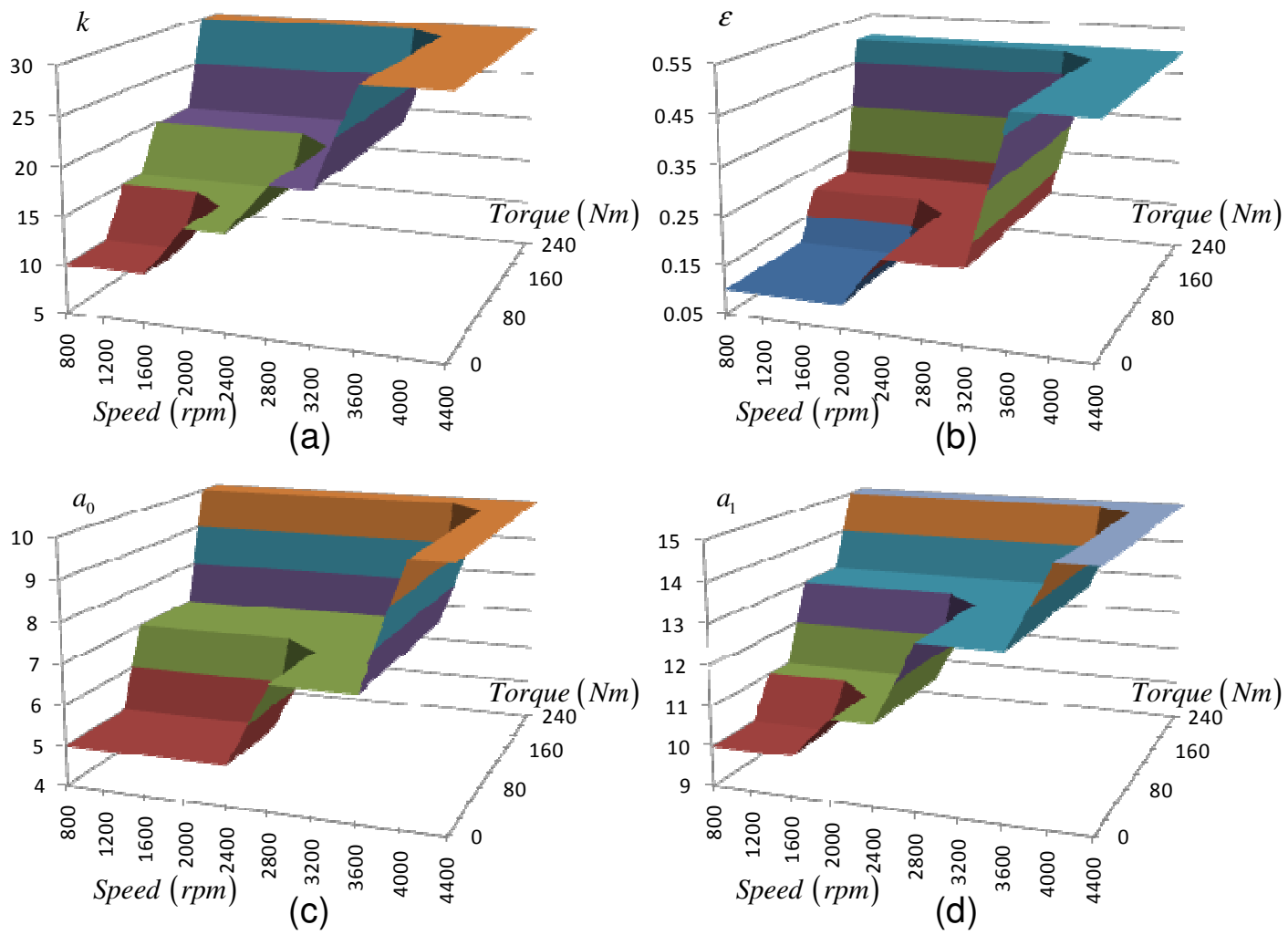

Figure 5: Several maps of design parameters in the sliding-mode control system. (a) k. (b) ε. (c) a_0. (d) a_1.

EXPERIMENTAL RESULTS

We implemented the control algorithm in Figure 3 with an engine test bed and a pick-up truck using the same engine model. The engine test bed was connected to an engine dynamometer, and the pick-up truck was connected to a chassis dynamometer. The engine was modified from a Toyota 2KD-FTV diesel engine to run

diesel-dual-fuel by injecting 375 kPa CNG to each of the four intake ports. The distance from the CNG injector to the port is kept as small as possible at 25 cm to reduce time delay.

The engine has four cylinders, each of 2.5 liters, sixteen intake and exhausted valves with double overhead cam shaft (DOHC), a turbocharger with an EGR valve and a throttle but without variable geometry turbine (VGT), and common-rail direct fuel injection system.

The OEM ECU was replaced with an ECU whose hardwares are mainly from National Instruments. All control algorithms were written in Labview graphical programming language. A desktop computer acts as a host to communicate with human operator and is connected to a target running Labview Realtime and FPGA modules.

The PID controller (1) was implemented with a low-pass filter $1/(0.1s+1)$. The PID gains and the dead-zone compensator output u_c are given in Figure 4. The sliding mode controller (5) was used with an augmented sliding surface (6). All gains are given in Figure 5.

We first discuss the experimental results from the pick-up truck, followed by the results from the engine test bed. The pick-up truck was commanded to follow the new European driving cycle (NEDC.) The whole cycle comprises four urban cycles, each of about 200 seconds, and a sub-urban cycle of about 500 seconds.

Figure 6 contains the results of applying the gain-scheduling integrator-augmented sliding-mode controller. In following the NEDC, Figure 6(a) shows the plots of the measured common-rail pressure p (in solid line) and the desired pressure p_d (in dash line.) Both are plotted versus time. Excellent tracking results were obtained for the whole NEDC. Figure 6(b) shows the plot of the PWM duty cycle percentage u versus time. Figure 6(c) shows the plot of the battery voltage versus time, and Figure 6(d) shows the plot of the diesel fuel temperature versus time. It can be seen from Figure 6(c) that the battery voltage is slightly decreasing, which directly affects the increasing trend of the PWM duty cycle percentage in Figure 6(b). This is because when the supply voltage is low, the controller must increase its effort to obtain the same plunger gate lift. Supply voltage is a main disturbance we found to the common-rail pressure system since it can vary with electrical usage in the truck. However, the sliding-mode controller seems to handle this disturbance well. Another important disturbance we saw is the diesel fuel temperature which shows an increasing trend as in Figure 6(d). Usually, higher diesel fuel temperature tends to increase the control effort u.

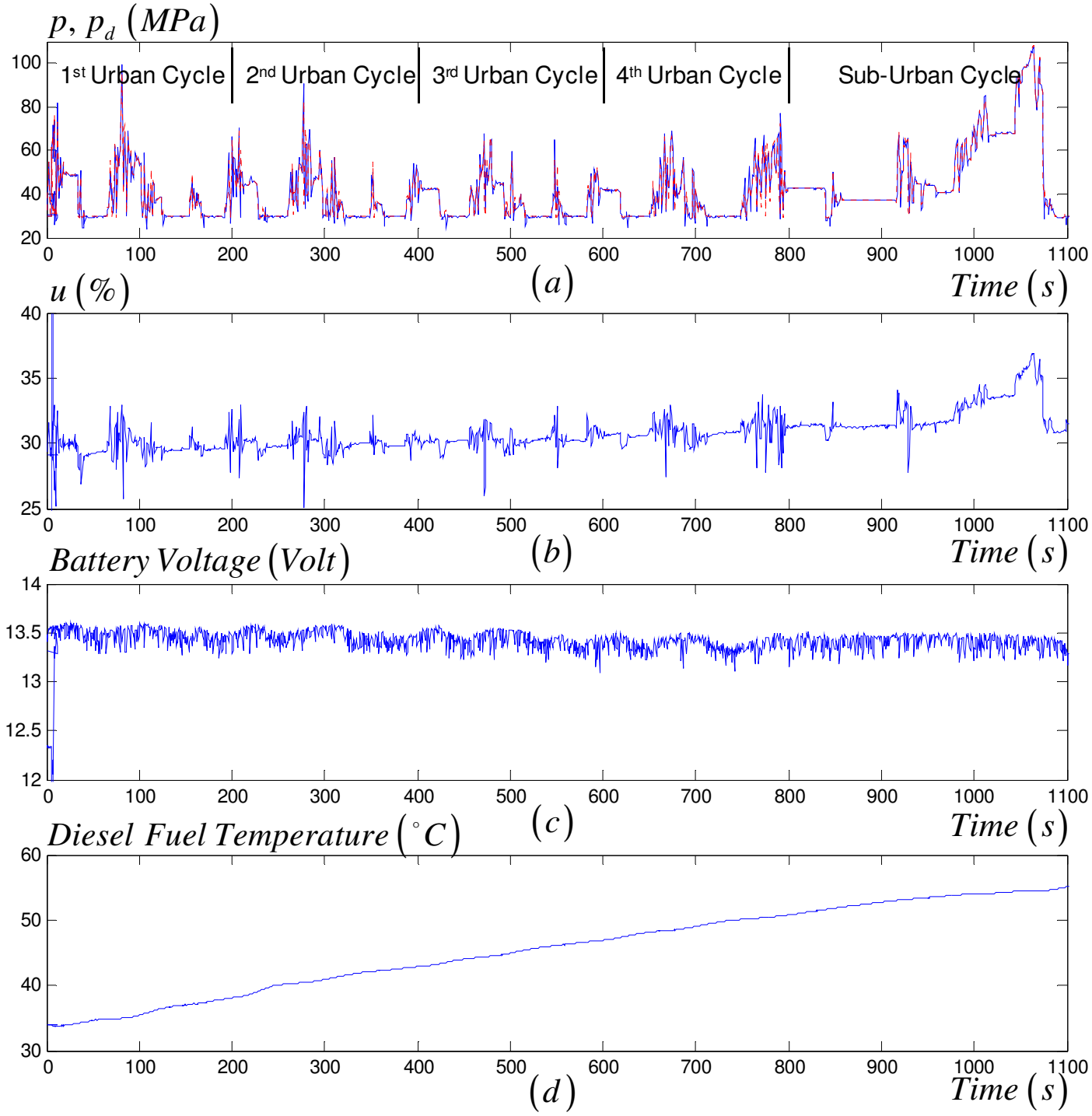

Figure 6: New European driving cycle test on a pick-up truck using the gain-scheduling integrator-augmented sliding-mode controller. (a) Measured rail pressure p (in solid line) and desired rail pressure p_d (in dash line.) (b) PWM duty-cycle percentage u to the pump's solenoid valve. (c) Truck battery voltage. (d) Diesel fuel temperature.

Figure 7 shows result of a road test using the PID controller. Figure 8 contains result of another similar road test using the proposed sliding mode control system. The driver tried to follow the same route using the same gear

and vehicle speed (as can be seen from the engine speed of both figures.) Comparing the results in both figures, the proposed sliding mode control system was able to follow well the swift desired pressure change demanded by the driver, better than the result from using the PID controller.

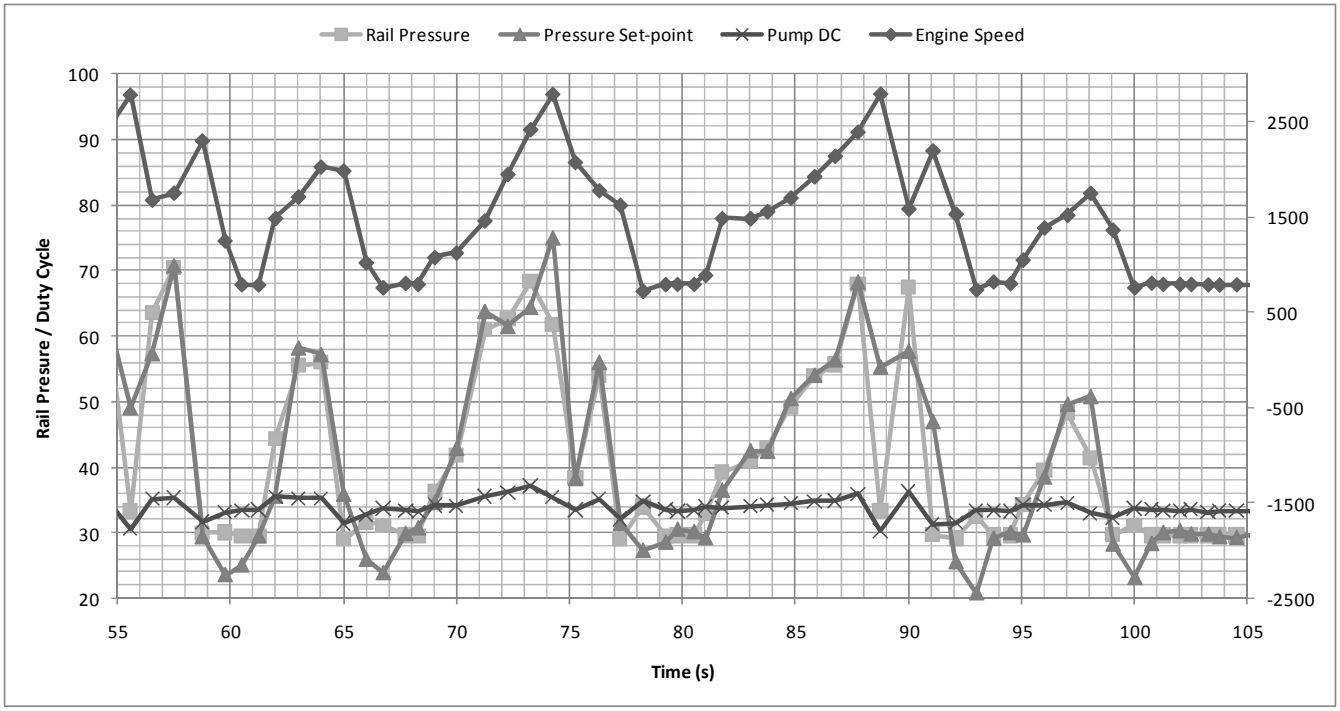

Figure 7: Road test on a pick-up truck using PID controller.

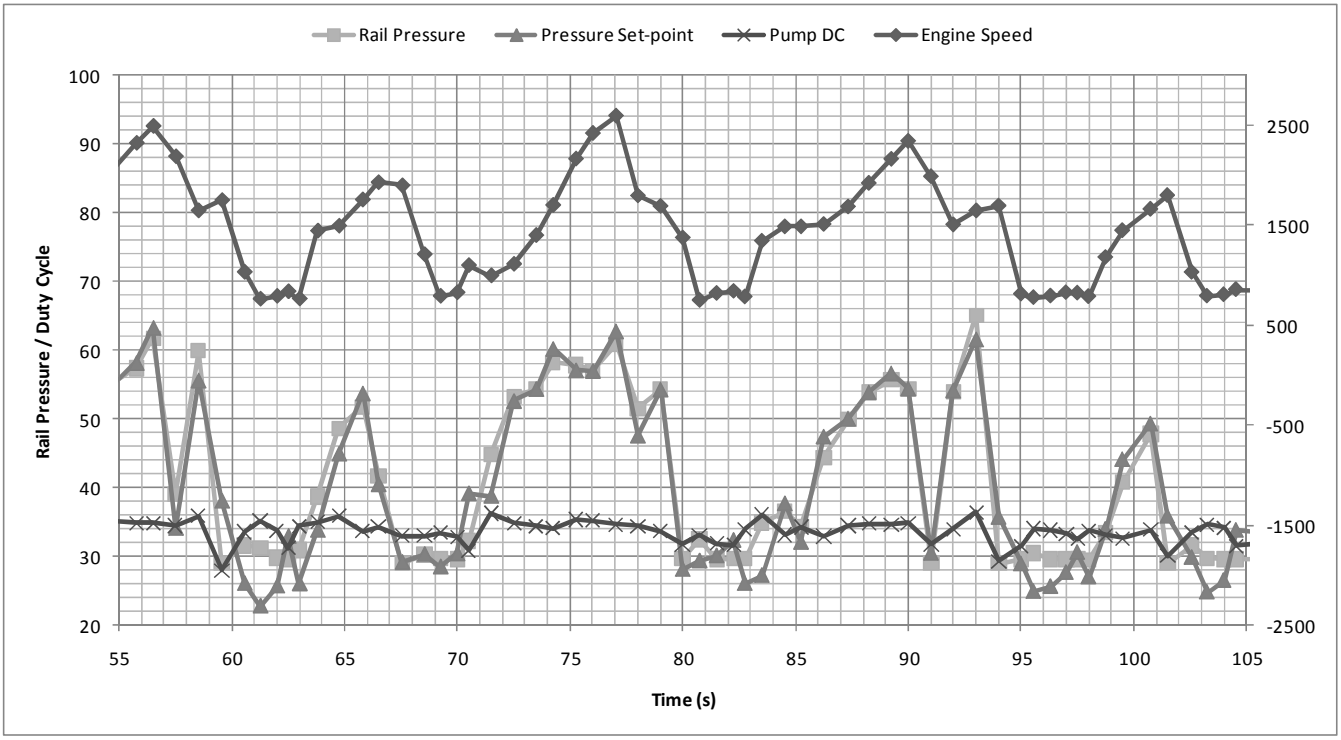

Figure 8: Road test on a pick-up truck using the gain-scheduling integrator-augmented sliding-mode controller.

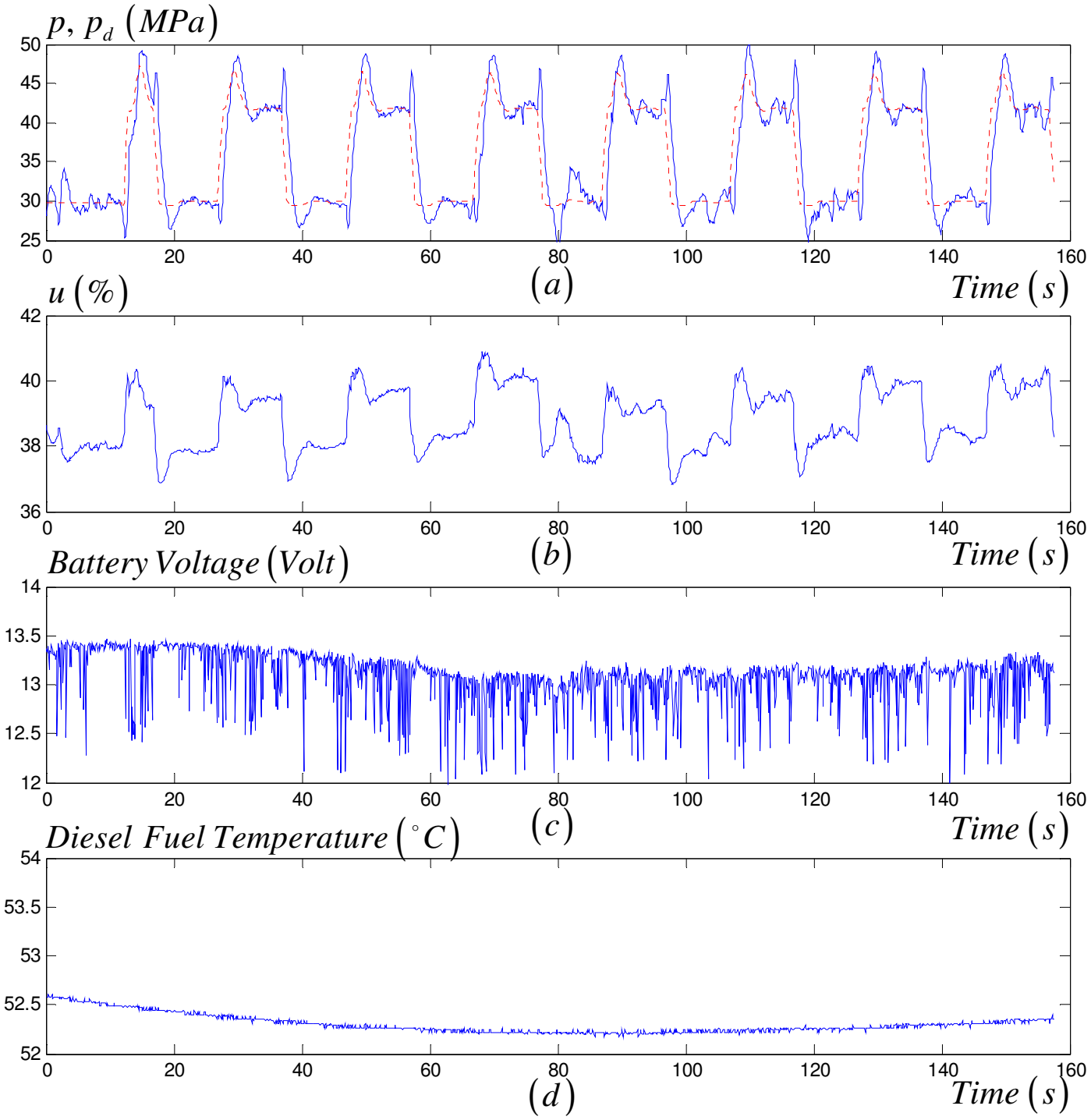

Figure 9: Set point changes test on an engine test bed using PID controller. (a) Measured rail pressure p (in solid line) and desired rail pressure p_d (in dash line.) (b) PWM duty-cycle percentage u to the pump's solenoid valve. (c) Battery voltage. (d) Diesel fuel temperature.

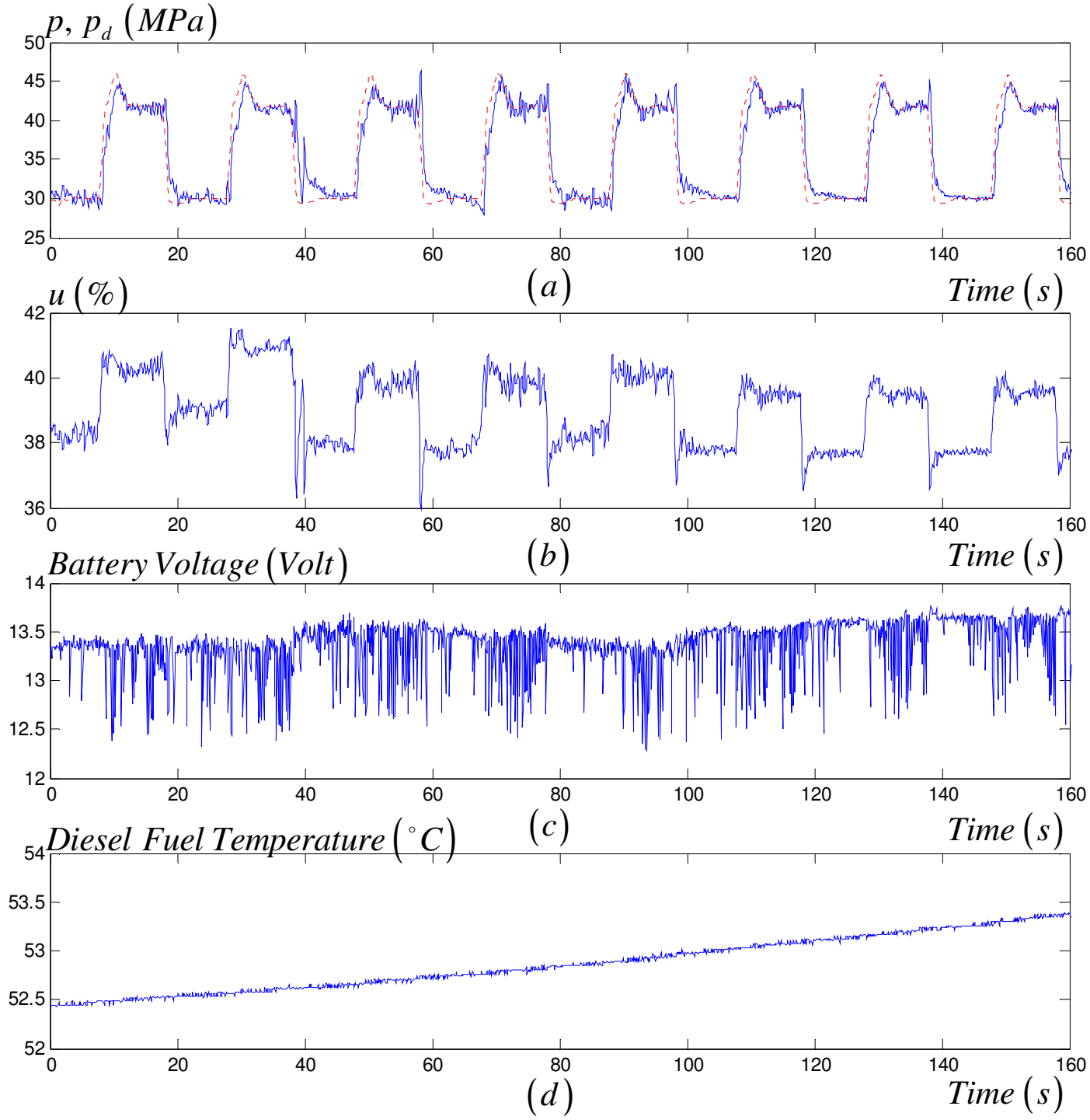

Figure 10: Set point changes test on an engine test bed using the gain-scheduling integrator-augmented sliding-mode controller. (a) Measured rail pressure p (in solid line) and desired rail pressure p_d (in dash line.) (b) PWM duty-cycle percentage u to the pump's solenoid valve. (c) Battery voltage. (d) Diesel fuel temperature.

Figure 9 includes the experimental results from the engine test bed using the PID controller. The measured common-rail pressure p was commanded to follow step changes in the desired pressure p_d. Figure 9(a) contains plots of the measured pressure (in solid line) and the desired pressure (in dash line) versus time. The measured pressure was unable to follow the desired pressure well, having both high overshoot and steady-state error. The lag between the desired pressure and the measured pressure can be seen as a result of the control system unable to react quickly enough with the desired pressure change. Figure 9(b) shows the plot of the PWM duty cycle percentage u versus time. Figure 9(c) shows the plot of the battery voltage versus time, and Figure 9(d) shows the plot of the diesel fuel temperature versus time. When the battery voltage dropped the most at around 70 to 80 seconds, the control effort u is at its highest point. During 120 to 160 seconds, even though the battery voltage slightly increases, the control effort u also slightly increases. This is because the diesel fuel temperature slightly increases as well, which counters the effect of the battery voltage.

Figure 10 contains the experimental results from the engine test bed using the proposed gain-scheduling integrator-augmented sliding-mode controller. From Figure 10(a), the measured pressure is able to follow closely the desired pressure with no overshoot and small steady-state error. Upon inspecting the control effort in Figure 10(b), more control chattering can be seen than that of Figure 9(b), resulting in more active control system. The effects of the battery voltage and the diesel fuel temperature to the control effort can be seen from Figure 10(c) and (d).

CONCLUSIONS

Due to its extensive operating range and different injection strategies, the diesel-dual-fuel engine is required to follow wide range of desired common-rail pressure. The disturbances from battery voltage and fuel temperature variations make tracking control using traditional PID controller, even with gain scheduling, difficult. The proposed sliding-mode control system has a dead zone compensator to compensate the dead zone effect, a gain-scheduling scheme to handle wide operating range, an augmented integrator for zero steady-state error, and a sliding-mode controller consisting of a reaching-phase continuous fast-acting controller for fast action and a sliding surface for good robustness. Together, the proposed control system was able to deliver excellent tracking results as seen from a pick-up truck following the NEDC and road test and an engine test bed by varying the desired pressure set point.

There are several tasks that can be performed in future researches. First is the improvement on the dead-zone compensator. Instead of using a calibrated map like ours, a mathematical model can be formulated for the dead zone and hysteresis, which are the two hard nonlinearities normally found in hydraulic solenoid actuator. This fixed model can be used to cancel the effect of the hard nonlinearities so that a linear plant model can be used to represent the common-rail system more accurately. This will open up the possibilities of using many effective linear model-based control techniques.

Second is the use of adaptive algorithms. Gain scheduling that we used can be viewed as a simple type of adaptive controllers. Some adaptive control algorithms can be used to adapt either controller or plant parameters over the changing operating points to always achieve good tracking performance. Some recursive system identification can be used to learn hard nonlinearities and to cancel their effects in a scheme called adaptive inverse control.

Third is improvement on the sliding mode algorithm itself. In the presence of model uncertainty, there is no guarantee of robustness during reaching phase. An integral sliding mode method presented in [9] can be applied to ensure robustness at all time. The trajectory dynamic during sliding phase can be viewed as pole-placement control, where in our case a_0 and a_1 were designed to place the poles at the stable left-half-plane region. More

elaborated controllers can be used in place of the pole-placement control to obtain better results during sliding phase.

REFERENCES

[1] Coppo, M. and Dongiovanni, C., "Experimental Validation of a Common-Rail Injector Model in the Whole Operation Field," *Journal of Engineering for Gas Turbines and Power*, **129**:596-608, 2007.

[2] Morselli, R., Corti, E., and Rizzoni, G., "Energy Based Model of a Common Rail Injector," presented at 2002 IEEE Int. Conf. on Control App, Glasgow, Scotland, September 2002.

[3] Hu, Q., Wu, S. F., Stottler, S., and Raghupathi, R., "Modelling of Dynamic Responses of an Automotive Fuel Rail System, Part I: Injector," *Journal of Sound and Vibration*, **245**(5):801-814, 2001.

[4] Wu, S. F., Hu, Q., Stottler, S., and Raghupathi, R., "Modelling of Dynamic Responses of an Automotive Fuel Rail System, Part II: Injector," *Journal of Sound and Vibration*, **245**(5):815-834, 2001.

[5] Lino, P., Maione, B., and Rizzo, A., "Nonlinear Modeling and Control of a Common Rail Injection System for Diesel Engines," *Applied Mathematical Modelling*, **31**:1770-1784, 1959.

[6] Balluchi, A., Bicchi, A., Mazzi, E., Vincentelli, A. S., and Serra, G., "Hybrid Modeling and Control of the Common Rail Injection System," *Int. Journal of Control*, **80**(11):1780-1795, 2007.

[7] An, S., Shao, L., "Diesel Engine Common Rail Pressure Control Based on Neuron Adaptive PID," 2008 IEEE International Conference on Cybernetics and Intelligent Systems Paper 4670956, 2008.

[8] Chatlatanagulchai, W., Wannatong, K., and Aroonsrisopon, T., "Robust Common-Rail Pressure Control for a Diesel-Dual-Fuel Engine Using QFT-Based Controller," 2009 SAE Powertrains, Fuels and Lubricants Conference Paper 2009-01-1799, 2009.

[9] Utkin, V., Guldner, J., and Shi, J., Sliding Mode Control in Electromechanical Systems, CRC Press, Florida, ISBN-0-7484-0116-4, 1999.

[10] Tao, G. and Kokotovic, P. V., Adaptive Control of Systems with Actuator and Sensor Nonlinearities, John Wiley and Sons, New York, ISBN 0-471-15654-X:7-28, 1996.

[11] Khalil, H. K., Nonlinear Systems, 3rd Edition, Prentice Hall, New Jersey, ISBN-13 978-0130673893, 2001.

CONTACT INFORMATION

Contact Withit Chatlatanagulchai at mailing address:

Department of Mechanical Engineering
Faculty of Engineering
Kasetsart University
50 Phaholyothin Road,
Bangkok 10900, Thailand

or email address: fengwtc@ku.ac.th

ACKNOWLEDGMENTS

Thanks are due to Nitirong Pongpanich for setting up the experimental hardware.